# Optical "snowblowing" of microparticles and cells in a microfluidic environment using Airy and parabolic wavepackets

Jörg Baumgartl*[a], Gregor M. Hannappel[a], David J. Stevenson[a], Michael Mazilu[a], Daniel Day[b], Min Gu[b], and Kishan Dholakia[a]

[a]SUPA, School of Physics and Astronomy, University of St. Andrews, St. Andrews, Fife KY16 9SS, UK;
[b]Centre for Micro-Photonics, Faculty of Engineering and Industrial Sciences, Swinburne University of Technology, Hawthorn, 3122, Victoria, Melbourne, Australia.

## ABSTRACT

The year 2007 witnessed the experimental realization of extraordinary laser beams termed Airy and parabolic beams. Surprisingly, these beams are immune to diffraction and in addition exhibit transverse acceleration while propagating. This peculiar property of both Airy and parabolic beams facilitates the clearance of both microparticles and cells from a region in a sample chamber through particle/cell transport along curved trajectories. We term this concept "Optically mediated particle clearing" (OMPC) and, alternatively, "Optical redistribution" (OR) in the presence of a microfluidic environment, where particles and cells are propelled over micrometer-sized walls. Intuitively, Airy and parabolic beams act as a form of micrometer-sized "snowblower" attracting microparticles or cells at the bottom of a sample chamber to blow them in an arc to another region of the sample. In this work, we discuss the performance and limitations of OMPC and OR which are currently based on a single Airy beam optionally fed by a single parabolic beam. A possible strategy to massively enhance the performance of OMPC and OR is based on large arrays of Airy beams. We demonstrate the first experimental realization of such arrays.

**Keywords:** Airy beam, parabolic beam, particle clearing, optical trapping, optical guiding, spatial light modulator, colloid, cell, microfluidics

## 1. INTRODUCTION

The pioneering studies of Ashkin *et al.*[1,2,3,4] established that micrometer-sized objects including microparticles, cells, viruses and bacteria can be trapped in a laser focus, a technique termed optical tweezing.[5] Subsequently, optical tweezing has become part of a rich class of optical micromanipulation techniques[6] including *e.g.* optical transfection of cells[7,8] and laser-induced microchemistry.[9] As well as using single tightly focused laser beams, emergent optical micromanipulation techniques rely on various advanced laser fields. For instance, interferometric optical tweezers[10] have proven useful in fundamental studies on phase transitions.[11] Another example refers to scanned laser beams based on acousto-optical deflectors which allow one to create *dynamic* and *quasistatic* custom optical landscapes.[12,13] Recently, holographic optical tweezers (HOTs) have come to prominence.[14,15] HOTs facilitate the creation of *static* arbitray optical landscapes based on the ability to shape laser beams both in amplitude and phase. The most prominent example of a shaped laser beam is the Bessel beam[16] which does not spread while propagating. This unusual property facilitates, for instance, simultaneous optical micromanipulation of cells in different planes,[17] cell separation through selective cell guiding,[18] realization of optical conveyor belts,[19] and subwavelength nanopatterning.[20] The Bessel beam has recently been accompanied by the Airy beam, a second type of non-spreading beam which surprisingly bends while propagating.[21,22,23,24,25] Shortly after its discovery, the Airy beam was used in novel applications in the fields of optical micromanipulation[26,27] and plasma physics.[28]

*E-mail: jb211@st-andrews.ac.uk, Telephone: +44 (0)1334 46 1605, Fax: +44 (0)1334 46 3104, http://www.st-andrews.ac.uk/~atomtrap

Optical Trapping and Optical Micromanipulation VI, edited by Kishan Dholakia, Gabriel C. Spalding, Proc. of SPIE Vol. 7400, 74001R · © 2009 SPIE · CCC code: 0277-786X/09/$18 · doi: 10.1117/12.826193

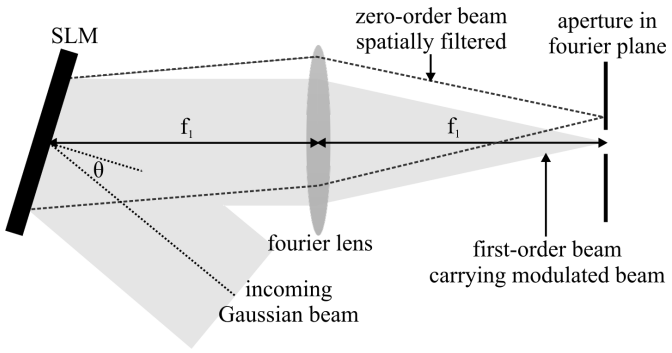


Figure 1. Conjugate-plane setup. The setup consists of a SLM and a fourier lens of focal length $f_1$ which is positioned at a distance of $f_1$ from the SLM. Due to this particular configuration, the complex laser beam amplitudes in the SLM plane and the back focal plane of the lens are mutually related via a fourier transform. In general, SLMs act as diffraction gratings because of the pixel structure. Therefore, a zero-order spot is inevitably present which carries approximately 10% of the incident intensity and which cannot be modulated at all. A linear grating (see Fig. 2(a)) is used to separate the first order spot from the zero order spot which is blocked by an aperture in the fourier plane. $\Theta < 10^\circ$ is the angle of incidence of the laser beam.

The novel applications of Airy beams within the field of optical micromanipulation are termed "Optically mediated particle clearing" (OMPC) and "Optical redistribution" (OR), or more evocatively as "Optical snowblowing", as used in the title of this paper. Both, OMPC and OR make use of the characteristic intensity pattern of Airy beams. This pattern consists of a bright main spot and a number of side lobes whose intensity increases towards the main spot. Therefore, microparticles and cells experience a gradient force which drags them into the main spot. Due to the light pressure exerted, microparticles and cells are then levitated and propelled along the curved trajectory of the main spot away from the cleared region. At a critical height, the Airy beam loses its non-spreading property. As a consequence, the beam profile blurs, and the gradient forces become weak. Microparticles and cells then drop out of the main spot and subsequently sediment back to the sample bottom in a region which is well separated from the cleared region. OMPC refers to this basic clearing effect[26] as opposed to OR which is associated with microparticle and cell redistribution between specially designed microwells.[27]

The present paper aims to provide a brief review of the work done on Airy beams and their application as micrometer-sized "snowblowers" for microparticles and cells. In addition, we explore strategies to enhance the quantitative performance of optical "snowblowing." We do not provide detailed descriptions and discussions of experimental aspects which are available in previous publications[26,27] and, in particular, on the web (free access).[29] The next section of this paper gives a brief introduction to HOTs based on spatial light modulators (SLMs) accompanied by an elucidation of the theoretical concept of Airy and parabolic beams, a second type of curved laser beams. The section is concluded by a brief description of the experimental realization of Airy and parabolic beams using a SLM. Then, we review the experimental demonstration of OMPC and OR in Sec. 3. In particular, we discuss the performance and limitations of the current approach which uses a time-shared combination of an Airy and a parabolic beam. The route to massively enhanced OMPC and OR is revealed in Sec. 4 where we introduce the idea of parallel arrays of Airy beams including first experimental realizations of such arrays. Finally, we conclude the paper in Sec. 5.

## 2. BASICS

### 2.1 Holographic optical tweezers and spatial light modulators

Holography refers to a technique where a reference laser beam illuminates a plate, the hologram, which either absorbs or refracts the incident beam in order to reconstruct a previously recorded 3D image. Absorbing and refracting holograms modulate both the amplitude and phase of the reference beam, respectively, and, therefore, are termed amplitude and phase holograms. HOTs work in a similar fashion, most commonly based on SLMs. Amplitude modulating SLMs consist of two crossed polarizers and a capacitor in between. The capacitor is filled with a twisted nematic liquid crystal (LC) which rotates the polarization of light incident on the SLM between

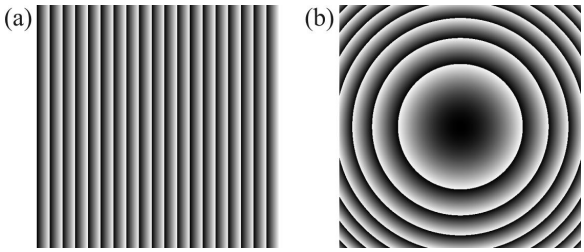


Figure 2. 8-bit gray-scale phase masks. The designated phase modulation of the laser beam is "wrapped" between $[0, 2\pi]$ and then converted into 8-bit gray-scale levels between $[0, 255]$ (0=black,255=white). These levels are finally rendered to voltages applied to the pixels of the SLM chip. The mask shown in Fig. (a) mediates a linear phase shift leading to a horizontal deflection of the incident laser beam. Figure (b) shows a quadratic phase modulation acting as a lens.

0 and 90 degree depending on the voltage applied to the capacitor. Accordingly, the intensity of the modulated light can be gradually adjusted between dark (no rotation) and bright (90 degree rotation). Phase-modulating SLMs consist of two parallel polarizers and a capacitor filled with a birefringent nematic LC aligned parallel to the polarization. This allows one to adjust the index of refraction (gradually between the ordinary and the extraordinary index) by tuning the voltage; as a consequence, the LC molecules are reoriented, and the phase of the incident beam is shifted between 0 and $2\pi$. Most SLM chips have a resolution between $800\,\text{pixel} \times 600\,\text{pixel}$ and $2000\,\text{pixel} \times 1000\,\text{pixel}$. Each pixel has a typical size of $8\,\mu\text{m} \times 8\,\mu\text{m}$ and is independently addressable to modulate a tiny fraction of the incident beam. The pixel structure imposes a limit on the efficiency of SLMs which act similar to a diffraction grating. As a consequence, a zero order spot is inevitably created which cannot be modulated at all, as opposed to the first order spot. Modern SLM devices deflect up to 90% of the incident intensity into the first order spot which is physically separated from the zero order spot as described below.

Phase-only SLMs are most commonly used in conjunction with a spherical lens, as sketched in Fig. 1. The distance between the SLM chip and the lens matches the focal length. As a consequence, the SLM plane and the back focal plane of the lens form a pair of conjugate planes, relating the associated complex amplitudes of the light fields to each other via a fourier transform. The conjugate plane configuration is the foundation of numerous scientific studies and applications in the fields of optical trapping, laser beam shaping, and imaging (see book chapter of Spalding *et al.* for an excellent elementary introduction and overview[15]). In particular, the conjugate plane configuration is of high relevance for the present work since it facilitated the creation of Airy and parabolic beams,[22,30] as briefly discussed in the next subsection.

Figures 2(a) and (b) show two elementary phase masks associated with deflection and focusing of the beam incident onto the SLM chip, respectively. Note that the imposed phase shift is "wrapped" between $[0, 2\pi]$ and then translated into 8-bit gray-scale values between $[0, 255]$. This grayscale image is converted to an array of voltages applied to the pixels of the SLM. The phase mask shown in Fig. (a) just imposes an overall linear phase shift which leads to a horizontal deflection of the incident beam. In Fig. (b), a quadratic phase shift is imposed which acts as a lens focusing the incident beam. Overall, these two basic phase masks allow one to relocate a laser focus in three dimensions at will.

### 2.2 Airy and parabolic beams: theory

The quantum-mechanical Schrödinger equation has an optical counterpart that is the paraxial equation of diffraction

$$\frac{\partial^2}{\partial x^2}\phi(x,y,z) + \frac{\partial^2}{\partial y^2}\phi(x,y,z) - 2i\frac{\partial}{\partial z}\phi(x,y,z) = 0. \tag{1}$$

$\phi(x,y,z)$ is the electric field envelope. $z$ is the propagation direction, and $x$ and $y$ are transverse coordinates. A particular solution of this differential equation is the Airy wavepacket

$$\phi(x,y,z) = \phi(x,z)\phi(y,z), \tag{2}$$

where

$$\phi_(\xi, z) = \mathrm{Ai}\left(\frac{\xi}{x_0} - \frac{z^2}{4k^2x_0^4}\right)\exp\left(i\left(\frac{\xi z}{2kx_0^3}\right) - i\left(\frac{z^3}{12k^3x_0^6}\right)\right), \quad \xi = x, y. \tag{3}$$

$x_0$ is a characteristic transverse length scale. At the origin, $z = 0$,

$$\phi(x, y, 0) = \mathrm{Ai}(x)\mathrm{Ai}(y) \tag{4}$$

This solution was first put forward by Besieris et al. in 1994.[21] The optical Airy wavepacket, or simply the Airy beam, is propagation invariant and, therefore, "non-diffracting". In addition, it exhibits transverse acceleration which is best represented by the lateral deflection

$$\Delta x(z) = \frac{z^2}{4k^2x_0^3}. \tag{5}$$

This expression directly follows from the argument of the Airy function in Eq. (3).

The Airy beam, as defined by Eqs. (2) and (3), could not be realized experimentally since it carries infinite intensity. This problem was finally solved in 2007 when Siviloglou *et al.* introduced a finite solution to Eq. (1) that is the exponentially apertured Airy beam, which may be simply considered as a finite Airy beam,[22,23]

$$\phi(\xi, z) = \mathrm{Ai}\left(\frac{\xi}{x_0} - \frac{z^2}{4k^2x_0^4} + i\frac{az}{kx_0^2}\right)\exp\left(\frac{a\xi}{x_0} - \frac{az^2}{2k^2x_0^4} + i\left(\frac{\xi z}{2kx_0^3}\right) - i\left(\frac{z^3}{12k^3x_0^6}\right) + i\left(\frac{a^2z}{2kx_0^2}\right)\right), \xi = x, y. \tag{6}$$

$a$ is the aperture coefficient. At the origin, $z = 0$,

$$\phi(x, y, 0) = \mathrm{Ai}(x)\mathrm{Ai}(y)\exp\left(\frac{a}{x_0}(x + y)\right). \tag{7}$$

In spite of the finite intensity, the finite Airy beam maintains its characteristic features, yet on a finite propagation distance. The Fourier transform of the finite Airy beam is

$$\widetilde{\phi}(k_x, k_y) \propto \exp(-ax_0^2(k_x^2 + k_y^2))\exp\left(\frac{i}{3}(x_0^3k_x^3 + x_0^3k_y^3 - 3a^2x_0k_x - 3a^2x_0k_y)\right) \tag{8}$$

This expression provides an intriguing result: in essence, finite Airy beams can be created through cubic phase modulation (terms $\propto k_x^3$ and $\propto k_y^3$) of a Gaussian laser beam (first exponential) using the conjugate plane setup described in Sec. 2.1 and Fig. 1. Note that the linear phase modulation in Eq. (8) just mediates a deflection of the incident Gaussian beam, as described in Sec. 2.1.

The discovery of Airy beams was followed by the theoretical study of parabolic beams.[31] Subsequent experimental realizations[30] of parabolic beams which also exhibit the main feature of Airy beams that is transverse acceleration is also of interest. Parabolic beams are further solutions of the paraxial equation of diffraction (1). A theoretical review of parabolic beams is beyond the scope of this paper, and the major differences between Airy and parabolic beams will become sufficiently clear below in Sec. 2.3. However, a proper discussion of the creation of parabolic beams requires the respective Fourier transforms which are

$$\widetilde{\phi}_n(k_x, k_y, z_0) \propto \exp\big(-ax_0^2(k_x^2 + k_y^2)\big)\Theta_n(\sqrt{2}x_0k_y)\exp\left(\frac{i}{3}(x_0^3k_x^3 - 3ax_0k_x + 3x_0^3k_xk_y^2)\right). \tag{9}$$

$n$ is a positive integer indicating the order of a parabolic beam. $\Theta_n$ denotes the $n$-th eigenfunction of the quartic oscillator which can be determined numerically.[32] Compared to Eq. (8), the eigenfunctions $\Theta_n$ imply an additional amplitude modulation of the incident Gaussian beam represented by the first exponential in Eq. (9). Note that parabolic beams also obey Eq. (5).

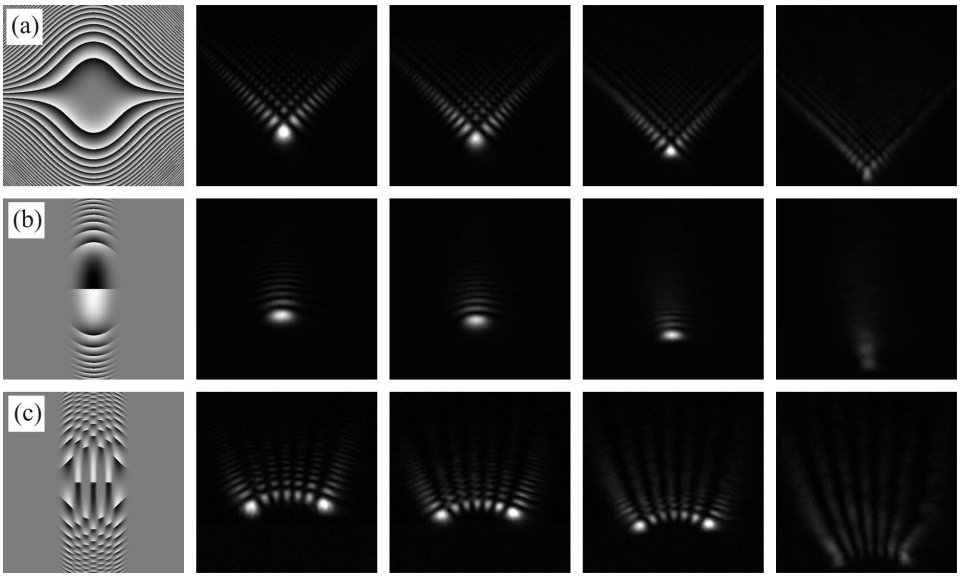


Figure 3. Airy and parabolic beams. (a) Left image: phase mask mediating a cubic phase modulation which, according to Eq. (8), allows one to create finite Airy beams using the conjugate plane setup shown in Fig. 1. The phase mask size is 600 pixel × 600 pixel. The remaining images in Fig. (a) show transverse beam intensity profiles at different propagation distances. If $f_1 = 500\,\text{mm}$ in Fig. 1, the propagation distance increases in steps of 2.7 cm in the series of images. The image size is $1.3\,\text{mm} \times 1.3\,\text{mm}$, the characteristic length is $x_0 \approx 32\,\mu\text{m}$, and the deflection is $x_d(z = 8\,\text{cm}) \approx 300\,\mu\text{m}$ (right image). Figure (b) shows on the left hand side the phase mask used to create $n = 0$ parabolic beams and subsequently a sequence of transverse beam intensity profiles. Similarly, Figure (c) shows the phase mask and beam intensity profiles for $n = 6$ parabolic beams. In general, $n = 0$ parabolic beams consist of a single main spot and a single tail of side lobes. $n > 0$ parabolic beams have two main spots and tails and $n - 1$ side tails in between as exemplarily shown for $n = 6$ in Fig. (b). This structure is mediated by the associated phase masks using a central row of $n + 1$ slices to modulate the incident beam.

### 2.3 Airy and parabolic beams: experimental realization

According to Eq. (8), a finite Airy beam is created through the cubic phase modulation of a Gaussian laser beam which is achieved using the experimental setup sketched in Fig. 1 and the cubic phase mask shown in the left image in Fig. 3(a). The four subsequent images in Fig. 3(a) show the created finite Airy beam at different propagation distances $z$ starting in the fourier plane where $z = 0$ (see Fig. 1). The beam consists of a bright main spot and a series of side lobes. The intensity of these lobes increases towards the main spot. Transverse acceleration manifests itself in the main spot moving downwards in the series of images. Intuitively, the Airy beam is referred to as a curved beam since the main spot follows a curve parabolic trajectory. During propagation the beam gradually blurs which is a consequence of the beam's finite nature.

In essence, the Airy beam phase mask is reduced to a central set of $n + 1$ slices to create a parabolic beam of $n$-th order. This is exemplarily demonstrated in the left images in Figs. 3(b) and (c) which show the phase masks associated with $n = 0$ and $n = 6$ parabolic beams, respectively. The corresponding beam intensities show that a $n = 0$ parabolic beam consists of a main spot similar to the Airy beam, but the pattern of side lobes is reduced to a single tail. The $n = 6$ parabolic beam exhibits two main spots and tails and five intermediate rows of side lobes (in general, $n - 1$ intermediate tails for parabolic beams of $n$-th order and $n > 0$). Clearly, parabolic beams experience transverse acceleration similar to Airy beams. Figure 4 shows parabolic beams of different order at $z = 0$, i.e., in the fourier plane (see Fig. 1). The series of images demonstrates a considerable increase of the total beam size with increasing order $n$ which is highly relevant for the quantitative control of particle clearing as described in Sec. 3.

The parabolic beam phase masks are derived from the fourier transform (9) by first "wrapping" the required phase modulation $\Phi(k_x, k_y) = (x_0^3 k_x^3 - 3a x_0 k_x + 3x_0^3 k_x k_y^2)/3$ between $[0, 2\pi]$ which is then simply multiplied

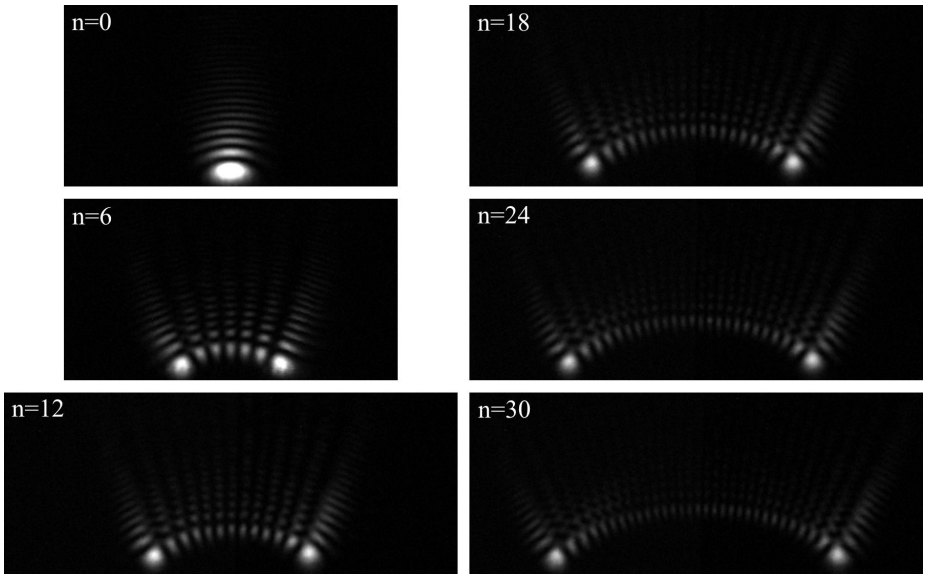


Figure 4. Parabolic beams of different order $n$. The series of images demonstrates the massive increase of the beam size with increasing order $n$. This allows one to quantitatively control the amount of redistributed microparticles and cells as discussed in Sec. 3.3.

by the required amplitude modulation $\Theta_n(\sqrt{2}x_0k_y)$. This approach is approximative but allows one to achieve amplitude modulation using a phase-only SLM operated in the conjugate plane configuration (see Fig. 1), as first demonstrated by Davis *et al.*[33] The approximative amplitude modulation causes ghost beams since the created parabolic beam is no longer the strict fourier transform of the modulated beam on the SLM chip. However, the ghost beams have a low intensity and, therefore, did not mediate any particle motion in the "snowblowing" experiments described in Sec. 3. In general, a strict simultaneous modulation of both amplitude and phase is possible, but demands the use of two SLMs or dual passage of a single SLM, one half of the chip performing the amplitude modulation and the other half performing the phase modulation.[34]

The free parameter of both Airy and parabolic beams is the characteristic transverse length scale $x_0$ which matches the distance between the beam's main lobe and the first neighboring side lobe divided by 2.25.[35] $x_0$ can be tuned through changing the total cubic phase modulation imposed on the incident Gaussian beam. For instance, a total cubic phase shift of $(k_x^3 + k_y^3)/3 = -20\pi \ldots 20\pi$ was imposed on 1.5 cm yielding $x_0 \approx 30\,\mu\text{m}$ using the conjugate plane setup (see Fig. 1) and $f_1 = 500\,\text{mm}$. The aperture coefficient $a$ depends on the ratio $\omega_0/x_0$ where $\omega_0$ is the waist of the incident Gaussian beam.[35] Accordingly, $a$ is increased if $x_0$ is decreased which results in a shorter propagation distance of finite Airy and parabolic beams, before they blur massively and diffraction takes over.

Both Airy and parabolic beams were successfully applied within optical micromanipulation, as described and discussed in the following.

## 3. OPTICAL "SNOWBLOWING"

### 3.1 Experimental setup

The conjugate setup allows one to create Airy and parabolic beams where typically $x_0 = 30\,\mu\text{m}$. With this, the transverse deflection (5) is $\Delta x \approx (5 \cdot 10^{-8}\,\mu\text{m}^{-1})z^2$ ($[z] = \mu\text{m}$) which means that the beam must propagate a distance $z \approx 15\,\text{mm}$ to achieve a deflection of $10\,\mu\text{m}$. Clearly, beams of that size and curvature are not useful to manipulate micrometre sized objects such as cells; the trapping forces would be too weak and object levitation too high in order to achieve precise "snowblowing". Therefore, the Airy and parabolic beams must be downsized which is achieved using an inverse telescope as shown in Fig. 5. The characteristic length for the downsized beam was $x_0 \approx 1\,\mu\text{m}$ in conjunction with a transverse deflection $\Delta x \approx (1.5 \cdot 10^{-3}\,\mu\text{m}^{-1})z^2$, i.e., $\Delta x \approx 10\,\mu\text{m}$

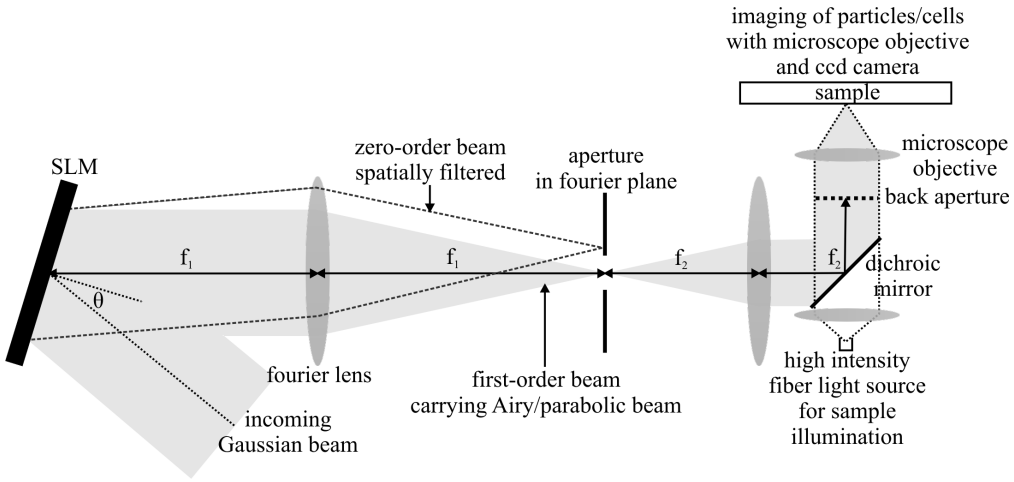


Figure 5. Typical HOTs setup for optical micromanipulation. The conjugate plane setup as shown in Fig. 1 is upgraded by a second lens of focal length $f_2$ and a microscope objective. The distances between the second lens and both the aperture in the fourier plane and the back aperture of the microscope objective match the focal length $f_2$. Therefore, the SLM plane and the sample plane form a pair of conjugate planes. In addition, the beam is always fully transmitted through the back aperture of the microscope objective if the beam is deflected within the fourier plane. Overall, this setup allows one to create micrometer-sized laser beams in the sample plane which can be relocated both transversely and vertically at will using the basic phase masks shown in Fig. 2. In particular, micrometer-sized Airy and parabolic beams can be created for "snowblowing" of microparticles and cells. The setup includes a high-intensity fiber light source to illuminate cells in the sample plane. Microparticles and cells are imaged using a microscope objective and a CCD camera. The setup can be implemented into an inverted microscope using the objective for both optical manipulation and imaging in reflection.

already for $z < 100\,\mu\text{m}$. Note that this setup maintains the conjugate plane configuration since the fourier plane is imaged from below into the sample plane. The fourier plane and the back aperture of the microscope objective form an additional set of conjugate planes. Therefore, the laser beam is always fully transmitted through the back aperture even if the beam is relocated within the fourier plane. Typical laser powers in the sample plane were 25 mW per beam.

Full experimental details of the "snowblowing" studies are described elsewhere (free access on the web[29]) and shall not be repeated in detail, here. Briefly, particles and cells in the sample plane were illuminated using a high intensity fiber light source and imaged from above onto the chip of a CCD camera using a microscope objective (20× or 50× magnification). The sample chamber consisted of two microscope cover slips and a stack of two vinyl spacers to achieve sample heights of approximately 100 µm. Then, microparticles and cells were not levitated to the top cover slip by the Airy and parabolic beams. Accordingly, the top cover slip did not have any influence on OMPC and OR, as studied in our experiments. Microwells were replicated using poly(dimethyl siloxane) (PDMS) and a negative, poly(methyl methacrylate) (PMMA) mold. The microwell structure was put onto the bottom cover slip of the sample, and microparticles or mammalian cells were added prior to sealing of the sample chamber with the second cover slip.

### 3.2 Results

Figure 6 shows how a combination of an Airy and a parabolic beam allowed us to redistribute microparticles between two microwells each $100\,\mu\text{m} \times 100\,\mu\text{m}$ in size and containing approximately 300 microparticles (polystyrene, diameter $\sigma = 5.7\,\mu\text{m}$). First, the pair of beams, an Airy beam fed by a $n = 24$ parabolic beam (see Fig. 7), was positioned close to the wall as indicated by the two rectangles in Fig. 6(a). The beams operated according to a time-shared protocol $\{t_1, t_2, t_{\text{off}}\}$: first, the Airy beam operated for $t_1 = 4\,\text{s}$ followed by the parabolic beam operating for $t_2 = 4\,\text{s}$. Finally, both beams were switched off for $t_{\text{off}} = 4\,\text{s}$ allowing levitated particles to drop out of the beam and to sediment back to the sample bottom. Figures 6(a)-(d) show how the beams had transported

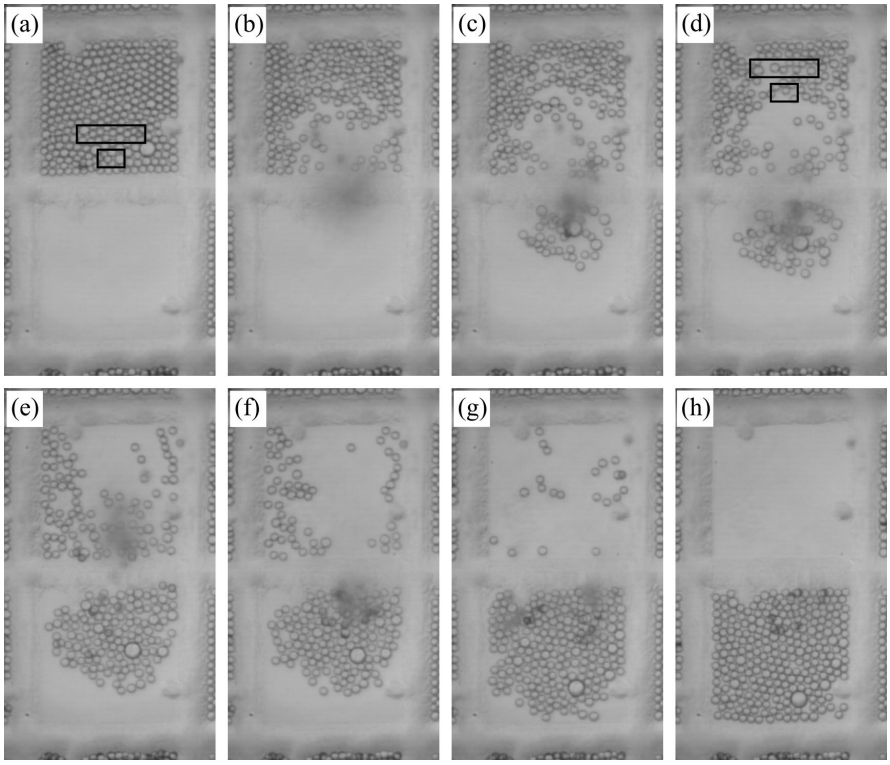


Figure 6. Optical redistribution of microparticles between microwells. (a) As indicated by the two rectangles, a pair of an Airy and a $n = 24$ parabolic beam (see Fig. 7) was positioned in front of the microwall. A time sharing approach was applied to aid particle escape from the main spots of the beams; first the Airy beam operated for $t_1 = 4\,\mathrm{s}$, and then the parabolic beam was switched on for $t_2 = 4\,\mathrm{s}$ followed by a cycle of $t_{\mathrm{off}} = 4\,\mathrm{s}$ where both beams were switched off. Figure (a) is the reference point for all the times $t$ mentioned in the following. (b)-(d) Situation after $t = 35\,\mathrm{s}$, $t = 70\,\mathrm{s}$, and $t = 105\,\mathrm{s}$ when the beams were relocated to a new region as indicated by the two rectangles. (e) Situation after $t = 3\,\mathrm{min}$. Particles were redistributed towards the wall. The beams were then relocated to the initial position as indicated in Fig. (a) to convey particles to the neighboring well. (f) Situation after $t = 6\,\mathrm{min}$. (g),(h) A single Airy beam was relocated across the compartment to collect and convey the remaining particles. (g) $t = 13\,\mathrm{min}$. (h) $t = 23\,\mathrm{min}$.

approximately 25% of the particles across the wall into the neighboring microwell. An additional two-step relocation of the pair of beams within the microwell facilitated to propel 90% of the particles to the neighboring compartment within a time span of $t = 6\,\mathrm{min}$, as shown in Figs. (d)-(f). Finally, the upper compartment was completely emptied by relocating single Airy beams and pairs of beams across the entire microwell. Figures (g) and (h) show the situation after $t = 13\,\mathrm{min}$ and $t = 23\,\mathrm{min}$, respectively. Overall, the series of images clearly demonstrates that curved beams allow one to precisely transport a large amount of particles between two microwells, notably without losing any particles. However, a limitation is revealed as well: it took only $t = 6\,\mathrm{min}$ to clear 90% of the particles, but an additional time of 20 min was required to sweep the remaing 10% of particles. This implies that optical redistribution of dilute systems of particles and cells requires a new strategie, beyond pairs of Airy and parabolic beams relocated across the region to be cleared. Section 4 briefly explores such a new possible strategy.

We have also demonstrated optical redistribution of mammalian cells which opens novel perspectives within the biological arena, in particular for the relocation of cells between different buffer media.[36] Figures 8(a)-(c) show how red blood cells are conveyed between two microwells. Note that the images were recorded at a higher magnification (50×) compared to the images shown in Fig. 6 where the magnification was 20×. In Fig. 8(b), the image apparatus was focused to a plane approximately 75 µm above the sample bottom; at this height, cells had already experienced a sufficiently large transverse deflection to sediment into the lower microwell after being released from the Airy beam. In general, the relocatable imaging apparatus allowed us to conveniently verify

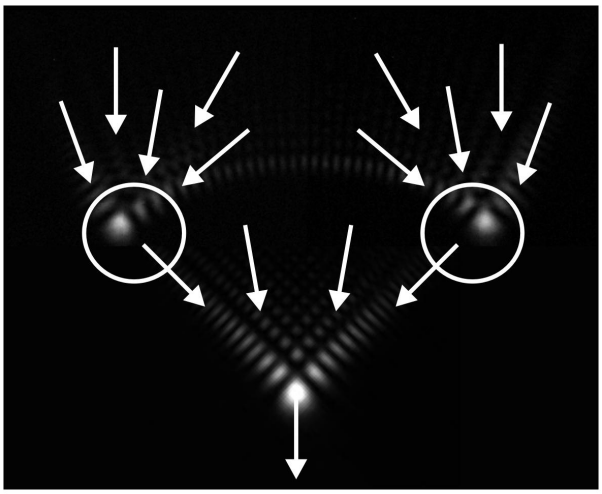

Figure 7. Beam configuration for particle redistribution. The upper beam, a $n = 24$ parabolic beam, collected particles (as indicated by the arrows) across the side lobes into the two main spots (indicated by circles) and subsequently conveyed particles along an arc-like trajectory towards the Airy beam shown below the parabolic beam. Then, the Airy beam dragged particles across the side lobes into the main spot which transported particles along a curved path similar to the parabolic beam. The beam configuration shown is the best compromise between quantitative control and efficiency of particle redistribution which is discussed below in Sec. 3.3 and, in particular, in Fig. 10.

particle and cell transport along curved paths. However, once verified, the optical redistribution does not require separate imaging optics, but instead can be implemented into an inverted microscope using the microscope objective for both focusing the laser beam into the sample and imaging. We have successfully observed particle clearing using an inverted microscope (Nikon TE2000).

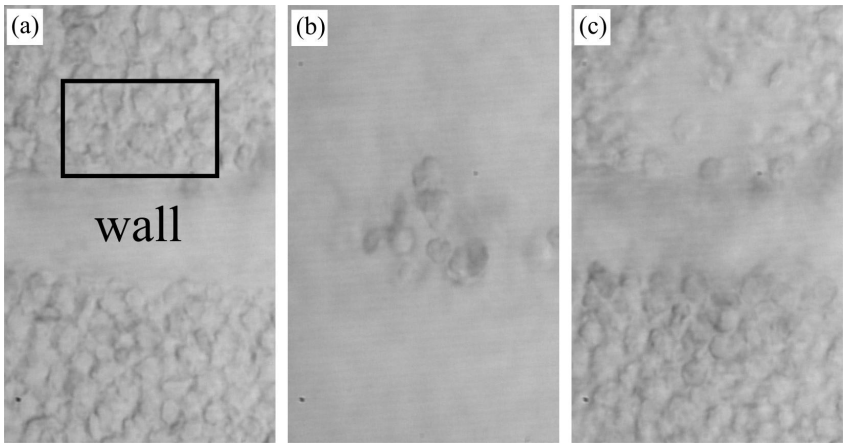


Figure 8. Optical redistribution of red blood cells between microwells. A single Airy beam oriented downwards was located in the area indicated by the rectangle in Fig. (a). The Airy beam dragged cells into the main spot, and cells were then propelled over the wall into the neighboring microwell. (b) Cells moved over the wall at a height of approximately 75 µm over the sample plane. (c) Situation after a minute: the upper microwell had been partially cleared from cells which reappeared in the lower microwell (see dark shade). Note that identical setup configurations were used for both the microparticle and cell experiments shown in Fig. 6 and here, respectively; however, cells were imaged with a higher magnification objective (50× instead of 20× for microparticles).

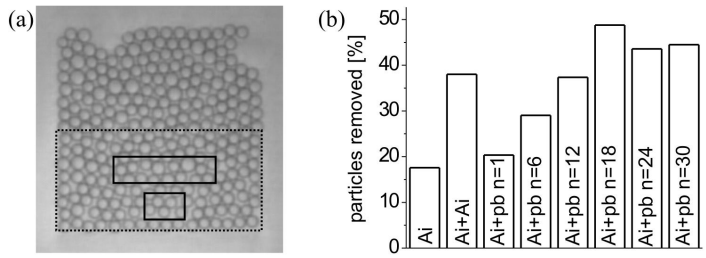


Figure 9. Efficiency of optical redistribution. (a) Experimental configuration: A single beam or a pair of beams was operating for ten cycles of first beam switch on for 4 seconds, then second beam switched on for 4 seconds, finally both beams switched off for 4 seconds. The amount of particles removed from the area indicated by the dashed rectangle served as a measure for the redistribution efficiency. An Airy beam was always operating within the area indicated by the lower solid rectangle. Apart from one reference measurement with a single Airy beam, either an Airy or a parabolic beam was located within the upper rectangle to feed the Airy beam. (b) Column diagram: number of removed particles for different beams and combinations of beams.

### 3.3 Quantitative control and efficiency of "optical snowblowing"

To investigate the efficiency of particle redistribution, we operated a combination of an Airy and a second beam (either Airy or parabolic beam) for ten cycles of $\{t_1, t_2, t_{\text{off}}\} = \{4\,\text{s}, 4\,\text{s}, 4\,\text{s}\}$. The amount of particles removed from an area comprising half a microwell (dashed rectangle in Fig. 9(a)) served as a measure for the redistribution efficiency. As a reference point, we also measured the efficiency of a single Airy beam. The results are summarized in Fig. 9(b). A single Airy beam removed just 20% of particles while a pair of Airy beams removed twice the amount. An Airy beam in conjunction with different parabolic beams allowed us to control the amount of removed particles between 20% and 50%. Very large parabolic beams ($n >= 24$), though, did not further increase the efficiency; in this case, the distance between the two main spots became considerably larger than the size of the Airy beam, which, as a consequence, was not efficiently fed with particles anymore. We have also found that the efficiency was lowered for time protocols which deviated from $\{t_1, t_2, t_{\text{off}}\} = \{4\,\text{s}, 4\,\text{s}, 4\,\text{s}\}$. Microparticle and cell transport then became imprecise as explained elsewhere.[27]

Overall, the combined pair of an Airy and a parabolic beam has proved a versatile tool to control particle and cell redistribution over a wide range. However, a question arises as to why single parabolic beams were not used to achieve this end goal. The answer is that parabolic beams turned out less efficient than Airy beams because of the following reason: both Airy and parabolic beams blurred while propagating due to their finiteness, which is

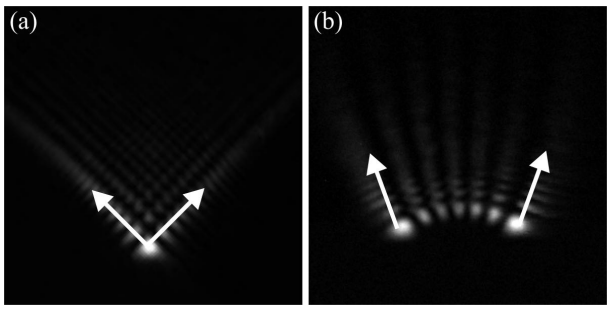


Figure 10. Efficiency of Airy and parabolic beams. Due to the finiteness, Airy and parabolic beams blurred while propagating which, after a certain beam propagation distance, enabled particles to leave the main spot in directions indicated by the arrows. (a) Particles and cells left the main spot at an angle of 45°. Therefore, particles and cells were still transported in the designated direction although with a lower efficiency. (b) Parabolic beams facilitated particle escape reversely to the designate direction which considerably lowered the efficiency.

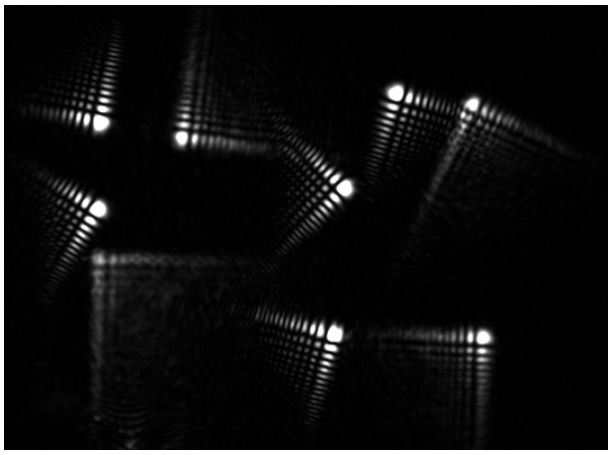

Figure 11. Multiple Airy beams. The superposition approach (10) is used to add or remove Airy beams at will. Some of the beams appear blurred since they were created in front of the fourier plane by imposing an additional square phase modulation (see Fig. 2(b)).

best seen in the beam intensity profiles on the right hand side of Fig. 3; the pattern of discrete lobes smeared out to a series of angular lines in the case of Airy beams and to parallel lines for parabolic beams. Along these lines, optical gradient forces became weak which enabled particles to leave the main spot. Clearly, this counteracted the lateral deflection of particles and cells which was necessary for efficient particle and cell clearing. However, the counteraction effect was less pronounced for Airy beams than for parabolic beams as highlighted by the arrows in Fig. 10. Particles and cells left the main spot at angles of 45° in the case of Airy beams and, therefore, were still transported in the correct lateral direction while further levitated by the main spot. In contrast, parabolic beams allowed particles to move reversely to the designated direction. As a consequence, many guided particles and cells fell back into the original microwell if parabolic beams were chosen to propel particles and cells over a wall into a neighboring microwell.

As well as the efficiency, the beam intensity made a major difference between Airy and parabolic beams. For the same intensity incident on the SLM, an Airy beam carried four times as much intensity than parabolic beams. This can be directly seen from the phase masks shown in Fig. 3(a)-(c). The cubic phase mask in Fig. (a) makes use of the entire SLM display and thus modulates the entire incident Gaussian beam. In contrast, the creation of parabolic beams only requires a central slice of the SLM chip (approximately 25% of the chip size). Accordingly, only a central slice of the incident Gaussian beam is modulated and transferred into the parabolic beam. Overall, the lack of both intensity and efficiency compared to Airy beams imposes a major limitation on the direct use of parabolic beams. Given the fact that Airy beams cannot just be made larger without decreasing their curvature, according to Eq. (5), a strategy for large-scale optical redistribution must overall be based on multiple Airy beams, as described in the following section.

## 4. ROUTE TO LARGE-SCALE "SNOWBLOWING": MULTIPLE AIRY BEAMS

Following a standard approach to create multiple traps,[15] multiple Airy beams were created by superimposing the complex fields of single Airy beams,

$$z = M \exp(i\Phi) = \sum_j \exp(i\Phi_j), \tag{10}$$

where $\Phi_j$ is the cubic phase modulation associated with the $j$-th Airy beam. This approach allowed us to create arbitrary arrays of Airy beams at will. New beams could just be added to the existing phase mask according to Eq. (10). In turn, single beams could be removed from the mask if the set of phases $\Phi_j$ is stored in memory. Figure 11 shows a set of multiple Airy beams that where created according to Eq. (10). A square phase (see Fig. 2(b)) was added to some of the beams which, therefore, were created in front of or behind the fourier plane

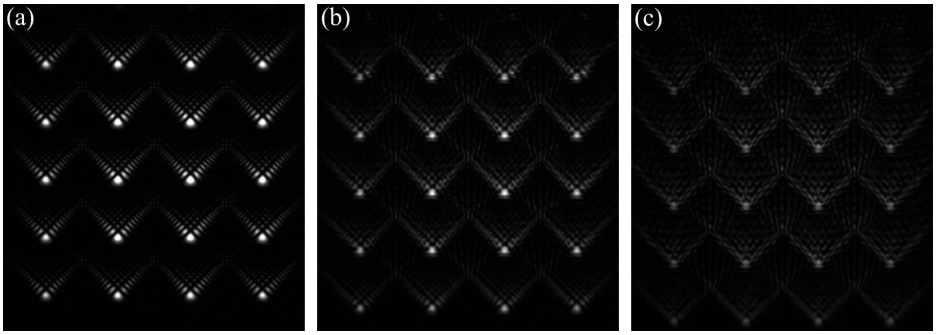


Figure 12. Parallel array of Airy beams at different propagation distances $z$. (a) $z = 0\,\mathrm{cm}$, (b) $z = 4\,\mathrm{cm}$, (c) $z = 8\,\mathrm{cm}$. The beams were created using the superposition approach (10) and the conjugate plane setup sketched in Fig. 1. The configuration of 20 parallel Airy beams is supposed to act as a large-scale "snowblower" propelling particles downwards.

where they appeared blurred. Figure 12 shows a regular pattern of parallel Airy beams at different propagation distances. We intend this pattern to act as a large-scale snowblower clearing large regions of samples.

The realized arrays of multiple Airy beams appear in accordance with predictions. However, the application of the beam arrays as large-scale "snowblowers" brings about a number of challenges. First, the approximative superposition approach (10) has both a fairly reduced efficiency and uniformity.[15] This is accompanied by the occurrence of strong ghost orders in the case of Airy beams. The ghost orders could be removed by accounting for the amplitude modulation $M$ in (10) as witnessed in our experiments (Note that all the images shown in Figs. 11 and 12 were actually obtained using amplitude modulation). However, preliminary experiments indicate a very poor efficiency since only 5 beams could be simultaneously used for particle clearing. Therefore, the efficiency must be increased using more advanced algorithms such as the Curtis-Koss-Grier algorithm.[15] A second challenge arises because multiple Airy beams mutually interfere which might modify the intensity pattern in a way that particle clearing becomes imprecise if not impossible. One way to avoid interference would be to control the polarization of the different Airy beams according to the approach by Preece *et al.*[37] which, however, would demand a more elaborate optical setup. In addition, it is unclear whether this approach would decrease the efficiency or not. Another possibility to avoid interference would be to apply a time-shared technique. Given that the beams are located on lattice sites, the total phase mask could be divided into four independent masks each covering one of the four possible combinations of odd/even sites in odd/even shells. The masks could be displayed at a rate of 60 Hz which should be fast enough to create quasistatic light forces to microparticles and cells.

## 5. CONCLUSIONS

We have successfully demonstrated OMPC and OR of both microparticles and cells using Airy and parabolic beams. The combination of an Airy and a parabolic beam of order $n$ allowed us to control the amount of cleared particles over a wide range. However, this approach is not suitable for clearing of large areas or dilute systems of microparticles and cells since relocation of the beams is time-consuming. Due to the limitations of parabolic beams with respect to efficiency and intensity, arrays of Airy beams are the most promising approach for large-scale "snowblowing". We have achieved the first realization of multiple Airy beams by superimposing the complex fields of single beams including amplitude modulation. The application of multiple Airy beams for OMPC and OR requires further efforts towards more efficient phase masks and time-shared approaches to avoid multiple-beam interference.

## ACKNOWLEDGEMENTS

We thank the UK EPSRC for funding. KD is a Royal SocietyWolfson Merit Award holder.

## REFERENCES


1. A. Ashkin, "Acceleration and trapping of particles by radiation pressure," *Phys. Rev. Lett.* **24**, pp. 156–159, 1970.
2. A. Ashkin, J. M. Dziedzic, J. E. Bjorkholm, and S. Chu, "Observation of a single-beam gradient force optical trap for dielectric particles," *Opt. Lett.* **11**, pp. 288–290, 1986.
3. A. Ashkin, J. M. Dziedzic, and T. Yamane, "Optical trapping and manipulation of single cells using infrared-laser beams," *Nature* **330**, pp. 769–771, 1987.
4. A. Ashkin and J. M. Dziedzic, "Optical trapping and manipulation of single cells using infrared-laser beams," *Science* **235**, pp. 1517–1520, 1987.
5. D. G. Grier, "A revolution in optical micromanipulation," *Nature* **424**, pp. 810–816, 2003.
6. K. Dholakia, P. J. Reece, and M. Gu, "Optical micromanipulation," *Chem. Soc. Rev.* **37**, pp. 42–55, 2008.
7. X. Tsampoula, V. Garcés-Chávez, M. Comrie, D. J. Stevenson, B. Agate, C. T. A. Brown, F. Gunn-Moore, and K. Dholakia, "Femtosecond cellular transfection using a nondiffracting light beam," *Appl. Phys. Lett.* **91**, p. 053902, 2007.
8. C. T. A. Brown, D. J. Stevenson, X. Tsampoula, C. McDougall, A. A. Lagatsky, W. Sibbett, F. J. Gunn-Moore, and K. Dholakia, "Enhanced operation of femtosecond lasers and applications in cell transfection," *J. Biophotonics* **1**, pp. 183–199, 2008.
9. D. McGloin, D. R. Burnham, M. D. Summers, D. Rudd, N. Dewara, and S. Anandc, "Optical manipulation of airborne particles: techniques and applications," *Faraday Discuss.* **137**, pp. 335–350, 2008.
10. M. M. Burns, J. M. Fournier, and J. A. Golovchenko, "Optical matter - crystallization and binding in intense optical fields," *Science* **249**, pp. 749–754, 1990.
11. J. Mikhael, J. Roth, L. Helden, and C. Bechinger, "Archimedean-like tiling on decagonal quasicrystalline surfaces," *Nature* **454**, pp. 501–504, 2008.
12. G. Milne, D. Rhodes, M. MacDonald, and K. Dholakia, "Fractionation of polydisperse colloid with acousto-optically generated potential energy landscapes," *Opt. Lett.* **32**, pp. 1144–1146, 2007.
13. D. Babic and C. Bechinger, "Noise-enhanced performance of ratchet cellular automata," *Phys. Rev. Lett.* **94**, p. 148303, 2005.
14. D. G. Grier and Y. Roichman, "Holographic optical trapping," *Applied Optics* **45**, pp. 880–887, 2006.
15. G. C. Spalding, J. Courtial, and R. D. Leonardo, *Structured Light and its Applications: An Introduction to Phase-Structured Beams and Nanoscale Optical Forces*, Academic Press, 2008.
16. J. Durnin, J. J. Miceli, and J. H. Eberly, "diffraction-free beams," *Phys. Rev. Lett* **58**, pp. 1499–1501, 1987.
17. V. Garcés-Chávez, D. McGloin, H. Melville, W. Sibbett, and K. Dholakia, "Simultaneous micromanipulation in multiple planes using a self-reconstructing light beam," *Nature* **419**, pp. 145–147, 2002.
18. L. Paterson, E. Papagiakoumou, G. Milne, V. Garcés-Chávez, S. A. Tatarkova, W. Sibbett, F. J. Gunn-Moore, P. E. Bryant, A. Riches, and K. Dholakia, "Light-induced cell separation in a tailored optical landscape," *Appl. Phys. Lett.* **87**, p. 123901, 2005.
19. T. Čižmár, V. Garcés-Chávez, K. Dholakia, and P. Zemanek, "Optical conveyor belt for delivery of submicron objects," *Appl. Phys. Lett.* **86**, p. 174101, 2005.
20. E. McLeod and C. B. Arnold, "Subwavelength direct-write nanopatterning using optically trapped microspheres," *Nature Nanotech.* **3**, pp. 413–417, 2008.
21. I. M. Besieris, A. M. Shaarawi, and R. W. Ziolkowski, "Nondispersive accelerating wave-packets," *Am. J. Phys.* **62**, pp. 519–521, 1994.
22. G. A. Siviloglou, J. Broky, A. Dogariu, and D. N. Christodoulides, "Observation of accelerating airy beams," *Phys. Rev. Lett.* **99**, p. 213901, 2007.
23. G. A. Siviloglou and D. N. Christodoulides, "Accelerating finite energy airy beams," *Opt. Lett.* **32**, pp. 979–981, 2007.
24. I. M. Besieris and A. M. Shaarawi, "A note on an accelerating finite energy airy beam," *Opt. Lett.* **32**, pp. 2447–2449, 2007.
25. G. A. Siviloglou, J. Broky, A. Dogariu, and D. N. Christodoulides, "Ballistic dynamics of airy beams," *Opt. Lett.* **33**, pp. 207–209, 2008.

26. J. Baumgartl, M. Mazilu, and K. Dholakia, "Optically mediated particle clearing using airy wavepackets," *Nature Photon.* **2**, pp. 675–678, 2008.
27. J. Baumgartl, G. M. Hannappel, D. J. Stevenson, D. Day, M. Gu, and K. Dholakia, "Optical redistribution of microparticles and cells between microwells," *Lab Chip* **9**, p. 13341336, 2009.
28. P. Polynkin, M. Kolesik, J. V. Moloney, G. A. Siviloglou, and D. N. Christodoulides, "Curved plasma channel generation using ultraintense airy beams," *Science* **324**, pp. 229–232, 2009.
29. http://www.rsc.org/suppdata/LC/b9/b901322a/b901322a.pdf.
30. J. A. Davis, M. J. Mintry, M. A. Bandres, and D. M. Cottrell, "Observation of accelerating parabolic beams," *Opt. Express* **16**, pp. 12866–12871, 2008.
31. M. A. Bandres, "Accelerating parabolic beams," *Opt. Lett.* **33**, pp. 1678–1680, 2008.
32. K. Banerjee, S. P. Bhatnagar, V. Choudhry, and S. S. Kanwal, "Anharmonics oscillator," *Proceedings of the Royal Society of London. Series A, Mathematical and Physical Sciences* **1703**, pp. 575–586, 1978.
33. J. A. Davis, D. M. Cottrell, J. Campos, M. J. Yzuel, and I. Moreno, "Encoding amplitude information onto phase-only filters," *Appl. Opt.* **38**, pp. 5004–5013, 1999.
34. A. Jesacher, C. Maurer, A. Schwaighofer, S. Bernet, and M. Ritsch-Marte, "Full phase and amplitude control of holographic optical tweezers with high efficiency," *Opt. Express* **16**, pp. 4479–4486, 2008.
35. J. E. Morris, M. Mazilu, J. Baumgartl, T. Čižmár, and K. Dholakia, "Propagation characteristics of airy beams: dependence upon spatial coherence and wavelength," *submitted* , 2009.
36. E. Eriksson, J. Enger, B. Nordlander, N. Erjavec, K. Ramser, M. Goksör, S. Hohmann, T. Nyström, and D. Hanstorp, "A microfluidic system in combination with optical tweezers for analyzing rapid and reversible cytological alterations in single cells upon environmental changes," *Lab Chip* **7**, pp. 71–76, 2007.
37. D. Preece, S. Keen, E. Botvinick, R. Bowman, M. Padgett, and J. Leach, "Independent polarisation control of multiple optical traps," *Opt. Express* **20**, pp. 15897–15902, 2008.